Dispersions of Zirconia nanoparticles close to the phase boundary of surfactant-free ternary mixtures

Andrea Fiorati,[a,b] Federico Florit,[a] Andrea Mazzei,[a] Stefano Buzzaccaro [a] Barbara Rossi,[c,d] Roberto Piazza,[a] Renato Rota[a] and Luigi De Nardo.[a,b]*

[a] Politecnico di Milano, Department of Chemistry, Materials and Chemical Engineering "G. Natta".

[b] INSTM - Local Unit Politecnico di Milano.

[c] Elettra Sincrotrone Trieste, Strada Statale 14 km 163.5, Area Science Park, 34149 Basovizza, Trieste, Italy.

[d] Department of Physics, University of Trento, Via Sommarive 14, 38123 Povo, Trento, Italy

Abstract The achievement of a homogeneous dispersion of nanoparticles is of paramount importance in supporting their technological application. In wet processing, stable dispersions were largely obtained via surfactant or surface functionalization: although effective, the use of dispersant can alter, or even impair, the functional properties of the resulting nanostructured systems. Herein, we report a novel integrated modelling and experimental approach to obtain stable ZrO_2 Nanoparticle (NP) dispersions at native dimensions (about 5 nm) in homogeneous ternary mixtures of solvents (*i.e.* water, ethanol, and 1,2-dichlorobenzene) without any further surface functionalization. A miscibility ternary diagram was computed exploiting the universal quasi-chemical functional-group activity coefficient (UNIFAC) model, which was then experimentally validated. Dynamic Light Scattering (DLS) on these mixtures highlights that nanometric structures, resembling nano-emulsion droplets, form close to the mixture two-

phase boundary, with a size that depends on the ternary mixture composition. ZrO_2-NPs were then synthetized following a classic sol-gel approach and characterized by XRD and Raman spectroscopy. ZrO_2-NPs were dispersed in HCl and mixed with different mixtures of ethanol and 1,2-dichlorobenzene (DCB), obtaining homogeneous and stable dispersions. These dispersions were then studied by means of DLS as a function of DCB concentration, observing that the nanoparticles can be dispersed at their native dimensions when the mass fraction of DCB was lower than 60 %, whereas the increase of the hydrophobic solvent leads to the NPs' agglomeration and sedimentation. The proposed approach not only offers specific guidelines for the design of ZrO_2-NPs dispersions in ternary solvent mixture but can also be extended to other complex solvent mixtures in order to achieve stable dispersions of nanoparticles with no functionalization.

Introduction

Zirconium dioxide (ZrO_2) found widespread application as engineering ceramic due to its excellent mechanical strength and stiffness, amphoteric behaviour, high thermal stability, and dielectric properties.[1–4] The peculiar properties of ZrO_2 nanoparticles (ZrO_2-NPs) have been exploited in a range of applications, encompassing scratch-resistant coatings,[5] oxygen sensors for fuel cell,[3] humidity sensors[6], and heterogeneous catalysis.[7] ZrO_2 can occur in three different polymorphs at atmospheric pressure: the monoclinic phase (m-ZrO_2), which is the most stable at temperatures below 1400 K, the tetragonal (t-ZrO_2), which is stable in temperature range 1400 - 2700 K, and the cubic phase (c-ZrO_2), more stable at higher temperatures (2700-2950 K).[8] ZrO_2-NPs have the advantage that metastable polymorphs can be dimensionally stabilized at room temperature,[5,9,10] exploiting the different properties each crystalline phase possess.

The Brownian motion in dispersion of nanoparticles leads to collisions which causes agglomerations[11] that can be hindered through their electrostatic, steric, or electrosteric stabilization.[12] The main approach to obtain thermodynamically stable dispersions of ZrO_2-NPs involves surface functionalization with either surfactants, carboxylic acids with long aliphatic chains, polymers, or other small organic molecules. Due to the amphiphilic behaviour of ZrO_2-NPs, their dispersion in organic solvents generally requires an accurate tuning of the capping agent. Grote and co-worker,[13] for instance, achieved the stabilization of 10 nm ZrO_2-NPs in chloroform using hexanoic, decanoic, or dodecanoic acids, with molar ratio (zirconia/additive) up to 10 %. Similar results were obtained in tetrahydrofuran by using bifunctional silane coupling agents,[14] or ligands containing vinyl groups;[15] vinyl coated nanoparticles can even be dispersed in acrylate solution and co-polymerized with it.[16] Wang and co-workers, by means of Hansen solubility parameter analysis, investigated the dispersion behaviour of carboxylate-grafted ZrO_2-NPs in 25 different organic solvents, covering a wide range of polarity.[17,18] Interestingly, they found that the combination of triethanolamine with methacrylic acid broaden the range of compatible solvents from benzene to methanol.[17]

Even if effective in achieving the stabilization of nanoparticles in solvents, the use of additives can alter, by impairing or hindering, the final properties of the systems. Indeed, while surfactants can stabilize colloidal dispersions, they can also add chemical or physical functions to the colloid itself.[19] In addition, the chemical nature of dispersant strongly influences the surface chemical properties of zirconia nanoparticles.[20] As example, the surface treatment of nanoparticles in inorganic-organic composites lead to decreases of the optical properties.[21] Finally, the addition of different chemical agents alter the viscosity properties.[22] For these reasons, the development of new strategies to get homogeneous nanoparticle distribution, by avoiding surface capping or functionalization, represents an attractive challenge.[21]

Recently, the intrinsic behaviour of ternary mixture of solvents, composed by two almost immiscible components (water and a hydrophobic organic solvent) and one hydrotope,[23] has become of great interest for the scientific community.[24] Indeed, it is reported that when some ternary mixtures are close to the two-phase boundary, the formation of nanometric assemblies can be observed. These systems are commonly defined detergent-less microemulsions, surfactant-free microemulsions, or even ultraflexible microemulsions.[24–27] In this context, the potential application, *e.g.* solubilisation processes,[27] of these surfactant-free microemulsions still represent a little explored field.

In this work, we report a novel approach to obtain a thermodynamically stable dispersion of zirconia nanoparticles at native dimensions (about 5 nm) in ternary homogeneous mixtures of three different solvents: water, ethanol, and 1,2-dichlorobenzene (DCB). Since DCB is a hydrophobic solvent -and its miscibility with water is negligible- ethanol, acting as hydrotrope, was added to obtain homogeneous mixtures.[23] In order to establish the proper ratio between the solvents, a miscibility ternary diagram was computed by the means of the universal quasi-chemical functional-group activity coefficient (UNIFAC) model,[28] a group-contribution thermodynamic model for the estimation of the activity coefficient in mixtures taking into account non-idealities. Contrarily to other activity coefficient models (e.g., NRTL, UNIQUAC), the UNIFAC model only requires the knowledge of the species in the mixture.[29,30] For this reason, the UNIFAC model is widely applied for miscibility problems when few or no data is available for the analysed mixture. The computed miscibility diagram was validated empirically and analytically. The ratio between H_2O, ethanol, and dichlorobenzene was determined by ^{1}H-NMR analysis. Once a valid approach for the obtainment of macroscopically homogeneous ternary mixtures was assessed, ZrO_2-NPs were synthesized by adapting a classical non-aqueous sol–gel approach and characterized them by XRD and Raman spectroscopy. Despite these nanoparticles can be easily dispersed in aqueous HCl solution (0.1 M), homogeneous dispersions in pure non-polar solvents like DCB cannot be achieved. This issue was overcome by the employment of the ternary mixtures of solvents studied with the UNIFAC model.

ZrO_2-NPs were firstly dispersed in HCl 0.1 M and then mixed with proper amount of ethanol and DCB achieving the desired stable nanoparticle dispersions and their behaviour was then studied by means of Dynamic Light Scattering analysis as a function of 1,2-dichlorobenzene concentration.

Experimental

All chemicals were purchased from Sigma-Aldrich (Sigma-Aldrich, Italy) and used as received without further purification.

Miscibility studies on ternary mixtures of water, 1,2-dichlorobenzene and ethanol

UNIFAC model. The UNIFAC model considers each molecule as an ensemble of groups and all groups in each molecule can interact with the ones of other molecules, giving rise to the miscibility properties, expressed by means of activity coefficients. Proper parameters are used to describe the interaction between groups. These are collected in databanks[31] which are continuously expanded as more experimental evidence is collected. Currently, two sets of parameters are widely used, namely: the standard parameters set,[32] which is mainly applied for the equilibrium of a liquid and a vapour phase (VLE), and the Magnussen parameters set,[33] which is applied for the equilibrium of two liquid phases (LLE). In this work the considered mixtures are high-boiling and can give rise to two liquid phases in equilibrium. The Magnussen set of parameters (UNIFAC-LLE) is therefore used in the following. The UNIFAC-LLE model adopts the standard UNIFAC equations[28] and solely change the parameters used in the model. Furthermore, the temperature at which equilibrium is considered should range approximately between (10 and 40) °C, as the group-interaction parameters were evaluated mainly in this range.[33] The aim of the model is to find all the mixtures which lead to phase separation, as to obtain the mixability regions in a ternary diagram. To do so, all regions of the ternary diagram which lead to phase separation are computed via equilibrium calculations adopting the UNIFAC model. Detailed description of the UNIFAC model and the equations needed to compute the activity coefficient are

reported in the Supporting information. In the following the composition of the mixtures will be expressed using mass fractions:

$$\omega_i = \frac{MW_i x_i}{\sum_j^{NC} MW_j x_j} \quad (1)$$

where MW_i is the molecular weight of species i, x_i the molar fraction of species i, and *NC* the number of species in the system.

Experimental validation of the model. In the first case, the miscibility of the solvents was qualitatively evaluated by adding DCB to homogenous mixtures of ethanol and water as described in Table S3 of the Supporting Information, then the samples were visually inspected to observe phase separation phenomena and compared with the computed miscibility region. For quantitative validation of the model, 5 different solvent mixtures were prepared: after vigorous mixing, the samples were centrifuged (10 minutes at 2000 rpm), the two phases were accurately separated, then 80 mg of each phase was diluted in DMSO-d6 (0.750 mL) containing tetramethylsilane (TMS, 0.03 %) as internal standard, and the molar ratios of the solvents were measured by ^{1}H-NMR spectroscopy by integrating the solvents signals with respect to the internal standard. The molar ratios were successively converted in mass ratios.

^{1}H-NMR spectra were recorded on Bruker ARX 400 instrument operating at the ^{1}H resonance frequency of 400 MHz. Chemical shifts (d, ppm) are reported relative to tetramethylsilane (TMS) as the internal standard. All the spectra were recorded in DMSO-d6 at 305 K. Coupling constants (J) are reported in Hz.

As reported in literature[34], ^{1}H-NMR signals were attributed as follows: H_2O δ = 3.70 (bs, 2H); EtOH δ = 1.09 (CC<u>H</u>$_3$, t, 3H), 3.45 - 3.54 (CC<u>H</u>$_2$O, dq, 2H, *J* = 5.09, 6.99 and 14.06 Hz), 4.38 (O<u>H</u>, t, *J* = 5.09); DCB δ = 7.35 - 7.42 (CHC<u>H</u>CH, m, 2H), 7.60 - 7.66 (ClCC<u>H</u>C, m, 2H). Due to the high concentration of the samples, as consequence chemical shifts of EtOH and H_2O signals may show some drift.

Preparation of zirconia nanoparticles dispersion in ternary mixture

Synthesis of zirconia nanoparticles. The synthesis of nanoparticles was carried out by adapting non-aqueous sol–gel approach from literature,[35,36] all the reactions were conducted in sealed pyrex tube under air atmosphere. Zirconium(IV) n-propoxide solution (70 % in n-propanol, 3.5 mmol, 1.6 mL) was added to benzyl alcohol (BnOH, 10 mL) in a 50 mL pyrex tube under magnetic stirring. After sealing, the reactive mixture was heated at 200 °C and left react for 6 days. At the end of the reaction, the reactive mixture was cooled down to room temperature and the resulting suspension was centrifuged for 45 minutes at 4000 rpm. The collected white powder was washed twice by suspending it in absolute ethanol (20 mL) and centrifuging it for 45 minutes at 4000 rpm. After the washing 280 mg (2.3 mmol, y = 65 %) of zirconium oxide nanoparticles (ZrO_2-NPs) were obtained.

Dispersion in ternary mixtures preparation and characterization. ZrO_2-NPs in ternary mixture was prepared as follow. The proper amount of ethanol wet ZrO_2-NPs were dispersed in aqueous HCl (0.1 M) and then mixed for few minutes by magnetic stirring until the achievement of a homogeneous and clear stock dispersion, containing 9.4 g L^{-1} of nanoparticles. Then a small volume of this dispersion was diluted with other aqueous HCl (0.1 M), ethanol and 1,2-dichlorobenzene to achieve the mass ratios summarized in Table 1. For the preparation of 10 mL of TM1, *e.g.*, 119 μL of ZrO_2-NPs stock dispersion was diluted with 1.79 mL of HCl_{aq} (0.1 M), in a vial under stirring, then 7.10 mL (5.60 g) of EtOH was added, and finally 1.02 mL (1.33 g) of DCB dropped into the solution.

Table 1. Mass fraction, density, and viscosity of the ternary mixtures of solvents used for ZrO_2-NPs dispersions.

Mixture ID	ω_{DCB} (%)	ω_{EtOH} (%)	ω_{HCl} (%)	ρ (g mL^{-1})	η (mPa s^{-1})	n
TM1	15.07	63.61	21.32	0.889 ± 0.01	1.78 ± 0.06	1.3818
TM2	60.23	37.74	2.03	1.04 ± 0.02	1.24 ± 0.04	1.4542
TM3	82.15	16.84	1.01	1.17 ± 0.02	1.22 ± 0.04	1.5018

Characterization. Zirconia nanoparticles were characterized by X-Ray diffraction experiments (XRD), conducted with Panalytical Empyrean diffractometer using the Bragg Brentano geometry (Cu-Kα1 radiation; λ = 0.154056 nm). The X-ray diffraction patterns were collected at room temperature in 5-70° 2θ range (scan step size = 0.02°, scanning time as per step = 20 s). The measure was repeated 3 times in order to increase the signal-to-noise ratio.

Raman spectra were recorded on ZrO_2 NPs placed on a glass slide, in air, at room temperature using an integrated micro-Raman system (Horiba-Jobin–Yvon, LabRam Aramis). The exciting radiation at 632.8 nm provided by the emission of a He–Ne laser was focused onto the sample surface with a spot size of about 1 μm^2 through a 100X objective. The scattered radiation was analysed using a 46 cm focal length spectrograph equipped with a holographic grating with 1800 grooves mm^{-1} and a charge-coupled device (CCD) detector. The Rayleigh scattering was filtered through a narrow band edge filter. The resolution was set about 0.35 cm^{-1}/pixel. The Raman spectra were recorded on the same sample several times to ensure the reproducibility of the measurements and to exclude any possible photo-degradation effect.

The densities (ρ) at 25 °C of TM1, TM2 and TM3 were evaluated by weighing 5 mL of the mixtures previously measured in a calibrated flask; the viscosities (η) at 25 °C were measured by means of a modified Ubbelohde viscometer (all these measurements were repeated fivefold).

Dimensions of ZrO_2-NPs were determined by Dynamic light scattering (DLS) measurements, conducted on a Zetasizer Nano ZS instrument (Malvern, UK), at 25 °C and 632.8 nm, with an equilibration time of 120 s at scattering angle of 173°. After the synthesis, the ZrO_2-NPs were dispersed in aqueous HCl (0.1 M) achieving clear dispersions, which was then transferred to Suprasil™ quartz glass cuvette and directly analysed. The DLS measurements of the ternary mixtures were conducted on a custom-made Dynamic Light Scattering setup (wavelength = 532 nm, scattering angle = 90°) that allows a better characterization of the short-time dynamics of the sample. In addition, this setup is equipped with a special cell that allows an optimal filtration of the sample, which strongly reduce the presence of spurious artefacts in the intensity correlation function due to the presence of dust.

The concentration of ZrO_2 in the solutions were determined by Inductively Coupled Plasma-Optical Emission Spectrometry (ICP-OES, Perkin Elmer Optica 8300), the samples were analysed after a microwave assisted digestion with nitric acid (65 % in water, trace metal grade).

10 μL of the dispersion were deposited on a 200-mesh carbon-coated copper grid and dried under ambient condition before analysis. ZrO_2-NPs were analysed by transmission electron microscopy (TEM, Philips CM 200 field emission gun). High Resolution TEM (HR-TEM) was performed by using a 200 kV accelerating voltage. Low beam current densities and short acquisition times were adopted in order to avoid structural transformation during acquisition of HR-TEM images.

Results and discussion.

Miscibility studies on ternary mixtures of water, 1,2-dichlorobenzene, and ethanol. Due to its intrinsic chemical-physical properties, water is generally poorly soluble, or in some case virtually

insoluble, in nonpolar organic solvents like 1,2-dichlorobenzene (DCB). Indeed, when water and DCB are mixed together, they undergo phase separation.[37] This issue can be easily overcome by the addition of a proper amount of a third polar co-solvent, which is totally miscible with both the species. In this work ethanol (EtOH) was chosen as co-solvent to achieve homogeneous mixtures with high mass fraction of DCB suitable for obtaining ZrO_2-NP dispersions at their native size. While using high mass fraction of EtOH (*e.g.* $\omega_{EtOH} \gtrsim 0.6$), homogeneous solutions of the selected three solvents can be easily achieved, a reduction of the ethanol mass fraction below $\omega_{EtOH} \lesssim 0.6$ generally leading to phase separation.

To accurately predict the proper mass fraction of each solvent, the UNIFAC model was applied and its reliability was experimentally tested with two different approaches. The UNIFAC model was chosen because the solvent mixture is fully defined, but no phase-separation data was available for this specific mixture. Notably, the UNIFAC model only requires the knowledge of the structure of the chemicals involved, while other models (NRTL, UNIQUAC) would require an extensive experimental campaign aimed at finding the required model parameters.[29,30] Instead, the UNIFAC model does not require user-provided parameters. In order to apply this thermodynamic model, the molecules involved in the mixture should be described by groups of atoms which establish specific interactions between them as described by the model through proper group-interaction parameters. The set of equations defined in UNIFAC model section and in Supporting Information was numerically solved using the parameters reported in Table S1 and the phase diagrams reported in Figure 1 and Figure S13 were obtained.

The model correctly predicts the miscibility of ethanol and DCB and the insolubility of water in DCB. The zone below the continuous line in the ternary diagram is in fact a miscibility gap (Figure 1): all mixtures having a composition within this zone will always lead to phase separation. The model can predict the composition of the two phases which form after separation and they are represented in the diagram as dotted lines (tie lines). All mixtures, which composition lies on a tie line, will lead to the same composition of the two separated liquid phases.

The qualitative model validation was carried out as described in experimental validation of the model section. Figure 1 additionally reports the results of the validation procedure. The circles represent the ternary mixtures which results in homogeneous solutions, while crosses represent the ternary mixtures which undergo phase separation: in all cases, the applied UNIFAC model well describes the ternary solvent mixture in terms of phase separation. As a further quantitative confirmation, 5 different solvent mixtures were prepared to obtain phase separation (Table S4) and the phases mass fractions were measured by means of ^{1}H-NMR analysis (Figures S1-S12). The results of ^{1}H-NMR titration, reported in Table S4, and in Figure 1 as squares, show a good accordance with the predicted tie lines. The position of the aqueous (low DCB fraction) phases on the diagram is more correctly predicted than the organic (high DCB content) phases. The different isomers of DCB are significantly different between each other in their physical properties, *e.g.,* 1,4-dichlorobenzene is solid at ambient temperature. This means that complex interactions arise between DCB molecules, according to the position of the chlorine atoms on the aromatic ring. The used UNIFAC model does not take into account the position of the chlorine atoms in the molecule and, currently, no group contribution is available in literature for groups containing chlorine and aromatic carbons separated by 0, 1, or 2 further aromatic carbons.[31] The accuracy for the aqueous phase can be explained in the same manner; as the quantity of DCB is very low, the overall influence of the inaccuracy in describing DCB isomers becomes negligible. The aqueous phase is thus described as a mixture of water and ethanol with traces of an organic aromatic species (regardless its actual structure).

Overall, the UNIFAC model provided a satisfactory prediction of the miscibility properties of the selected mixture of solvents. Notably, this model can be used for any combination of solvents (not limited to relatively simple compounds as the ones used in this work) and for any number of components. The UNIFAC model can be adopted also for more complex ternary mixtures, such as those for which more than one binary mixture shoes a miscibility gap.[33] This model is thus a useful tool to screen possible

249 solvent mixtures (which could lead to phase-separation) for the subsequent dispersion of nanoparticles,
250 without the need to prepare a high number of solutions aimed only at finding the miscibility properties
251 of the proposed solvents.

252 As the nanoparticles are dispersed in HCl_{aq} (0.1 M), the same qualitative tests were run by using a 0.1
253 M aqueous solution of HCl instead of pure water. No macroscopic difference was observed in the
254 miscibility behaviour of the mixtures. Therefore, the addition of a small quantity of HCl does not produce
255 significant differences with respect to the case of pure water in terms of miscibility of the three solvents.
256 This result is consistent with the results presented by Lopian and co-authors, where they investigate the
257 effect of strong acid in ternary mixtures made of octanol/ethanol/water.[26]

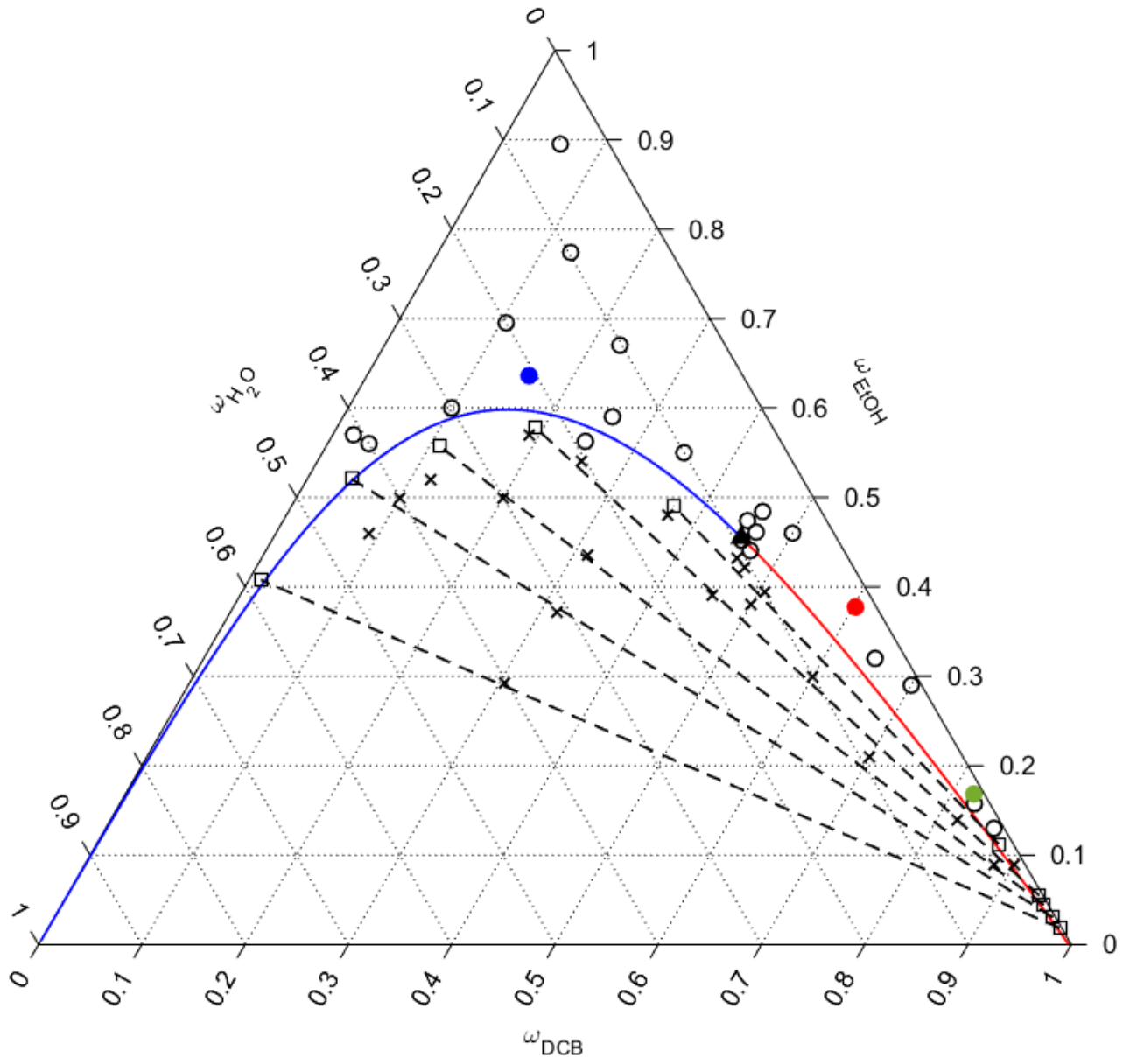

Figure 1. Ternary miscibility diagram of H_2O, ethanol, and 1,2-dichlorobenzene mixtures as computed from UNIFAC-LLE model. Continuous blue and red lines represent the boundaries of the mixability region (phase separation below these lines). Circles and crosses represent the qualitative empirical validation test. Circles indicate the mixtures which do not experimentally lead to phase separation, while crosses indicate mixtures which show phase separation. Squares indicate the mixtures prepared to determine the tie lines (dashed lines) as from ^{1}H-NMR. The three coloured circles (blue, red and green)

correspond to the composition of the three solvent mixtures discussed in Table 1, respectively TM1, TM2 and TM3. The black triangle is the predicted critical point of the mixability region. (colour figure online.)

Characterization and dispersion in acidic aqueous solution of ZrO_2 nanoparticles. The non-aqueous sol-gel synthesis of zirconium(IV) n-propoxide with BnOH results in ZrO_2 nanoparticles (NPs) with uniform size and both tetragonal (t-ZrO_2) and monoclinic (m-ZrO_2) phases:[38] the t/m-ZrO_2 ratio can be tuned by varying reaction temperature, constituent material of reactors (glass or Teflon®), and scale.[9] Indeed, the increase of the temperature up to 270 °C lead to higher amount of tetragonal phase in glass vessels, while the use of Teflon® reactor allow to achieve similar results at lower temperatures. The results here reported refer to the synthesis performed in sealed Pirex® glass tube at 200 °C, being the main scope of this work the achievement of homogeneous dispersions.

The crystal phase composition and the crystallite size of the obtained ZrO_2-NPs were quantified by performing Rietveld refinement (RR) on XRD diffractogram (Figure 1.a). RR was performed by means of Profex software[39] for recalculating the ICSD reference patterns of m-ZrO_2 (ICSD code: 98-008-0045) and t-ZrO_2 (ICSD code: 98-006-6789). The recalculated diffractogram (Figure 2.a), χ^2, and GOF (Table S5), indicate the quality of the fitting, the obtained values reliably providing the crystallite size, and the phase composition of the ZrO_2-NPs. The calculated weight fractions and the crystallite dimensions are reported in Table S5: results are consistent with previous published results; indeed Cheema and co-worker achieved, with the same synthetic approach at slightly higher temperatures, nanoparticles with 80 % of m-ZrO_2 fraction and crystallite dimension of about 5 nm.[9] The dominance of m-ZrO_2 phase was also confirmed by Raman spectroscopy, this technique being successfully employed to distinguish the ZrO_2 phases,[40–42] thanks to its sensitivity to the molecular environment. Indeed, as shown in Figure 2.b, in the Raman spectrum of collected nanoparticles, the signals attributed to m-ZrO_2 were predominant (177, 190, 223, 309, 331, 344, 381, 481, 503, 536, 560, 615, 619 and 631 cm^{-1}), while only the peaks at

145 and 277 cm^{-1} can be clearly attributed to t-ZrO_2 because all the others t-ZrO_2 signals (319, 472 and 646 cm^{-1}) appears only as shoulder of m-ZrO_2 peaks.[40–42]

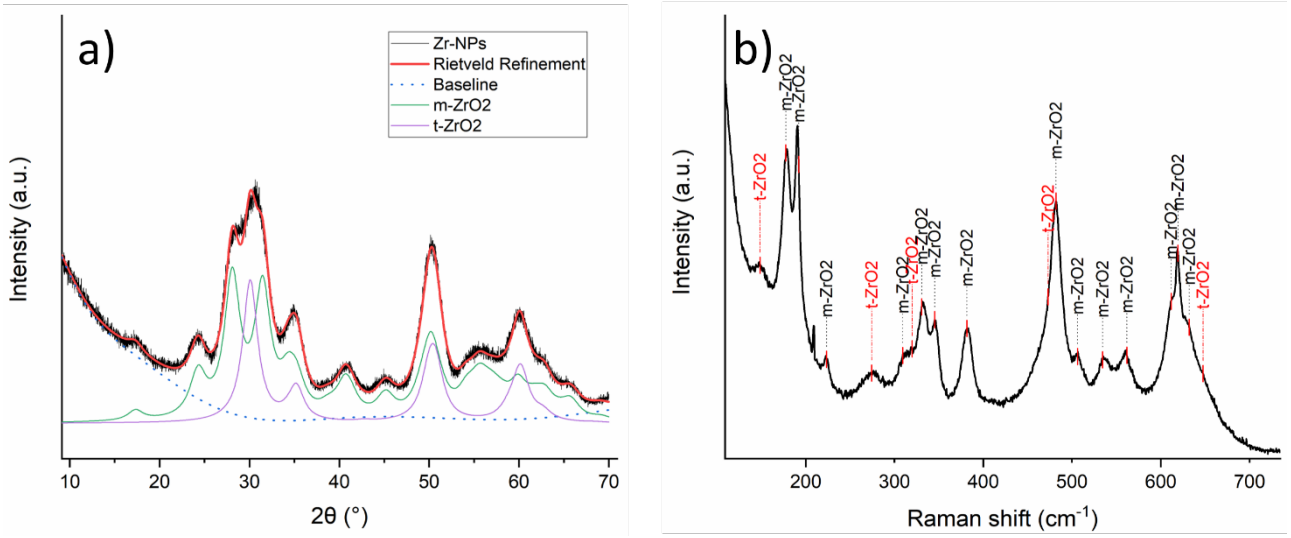

Figure 2. (a) XRD diffraction pattern and Rietveld refinement of ZrO_2-NPs, where: ZrO_2-NPs diffractogram (Black line), computed Rietveld Refinement (Red line), subtracted baseline (dashed blue line), m-ZrO_2 (green line computed), and t-ZrO_2 (purple line computed) XRD patterns. (b) Raman spectrum of ZrO_2-NPs collected using 633 nm of excitation wavelength.

ZrO_2-NPs have been easily dispersed in aqueous HCl 0.1 M simply by adding the powder to the acidic aqueous solution, resulting in a clear and transparent dispersion with concentration up to 9.4 g L^{-1}, without adding any dispersant. After appropriate dilution in aqueous HCl 0.1 M, DLS measurements (number distribution) showed a homogeneous particle size of this dispersion, resulting in a hydrodynamic diameter of about 5 nm (DLS, Figure 3 a). By analysing DLS measurements in terms of intensity distribution (Figure 3 b), it is possible to observe additional peaks, emphasizing the presence of larger aggregates with dimensions of hundreds of nanometres. DLS data is in fair accordance with crystallite size measured via XRD and Rietveld refinement (Table S4). Interestingly, this dispersion in water has been obtained without ZrO_2-NPs functionalization.

In order to widen the range of applications, ZrO_2-NPs generally need to be dispersed in organic solvents prior their use: for this reason, we investigated the possibility of preparing ZrO_2-NP dispersions in homogeneous ternary mixtures composed by water, 1,2-dichlorobenzene, and ethanol, avoiding any chemical modification of the nanoparticles surface. The proposed approach can be in principle extended to other organic solvents.

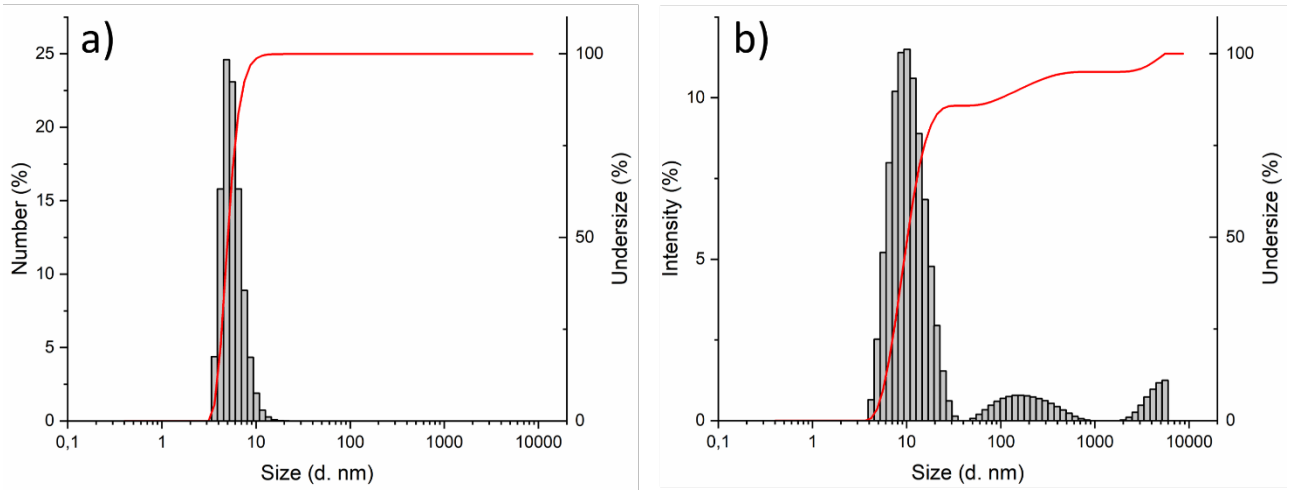

Figure 3. Particles size distribution of ZrO_2-NPs dispersed in aqueous 0.1 M HCl. (a) Data expressed in number of NPs *vs*. Size, (b) Data expressed in intensity of scattered light *vs*. Size. Grey bars represent the population frequency, red line the cumulative size distribution. (Colour figure online.)

DLS tests of nanoparticle dispersibility in ternary mixtures. With the aim of exploiting whether the zirconia nanoparticles can be dispersed into a non-aqueous solvent, we choose to approach the lower-right corner of the phase diagram in Figure 1 by following a path that borders the mixture two-phase boundary. Specifically, we made a detailed DLS test of the dispersibility and stability of the ZrO_2 nanoparticles at a concentration of about 0.11 g L^{-1} in the three solvents indicated by the blue, green, and red dots in Figure 3, whose compositions can be found in Table 1.

Before discussing the DLS result, it is useful to point out that a comparison of the visual appearance and time evolution of the three zirconia dispersions already highlights noticeable differences. Indeed, while TM1 and TM2 are transparent, without any evident flocculation up to several weeks since preparation, sample TM3 rapidly shows the formation of a sediment at the bottom of the cuvette. Visual evidence seems therefore to suggest that a consistent fraction of NPs may remain dispersed even upon a reduction of the water content to about 2 % in weight (solvent TM2). On the other hand, the rapid settling observed in sample TM3, whose water content is not much lower, seems to imply that, to keep stable the dispersion, the presence in the solvent of a substantial fraction of a polar component (like ethanol) is needed.

A more quantitative assessment of the previous considerations can be obtained by DLS. Yet, the analysis of scattering data from the investigated dispersions is not trivial because, rather surprisingly, the selected solvents significantly contribute both to the scattered intensity and to the decay of the DLS correlation functions. A straightforward reconstruction of the particle size distribution similar to the one shown in Figure 2 would in fact suggest the presence of scatterers that are consistently *smaller* than the original NPs. Hence, we regarded as useful to perform a DLS investigation of the ternary solvents mixtures used for the dispersions (TM1, TM2 and TM3). As shown in Figure 4, the correlation functions for the solvent mixtures decay on a time scale of a few microseconds, which is far larger than those typical of simple liquid mixtures. Notably, $g_2(\tau)$ is similar for the three solvent compositions investigated, and can reasonably be fitted as a single exponential, $g_2(\tau) - 1 = \exp(-\tau/\tau_r)$, with the same characteristic time $\tau_r \simeq 2.4\ \mu s$ for both TM1 and TM2, and $\tau_r \simeq 3.5 \mu s$ for TM3 (Figure 4).

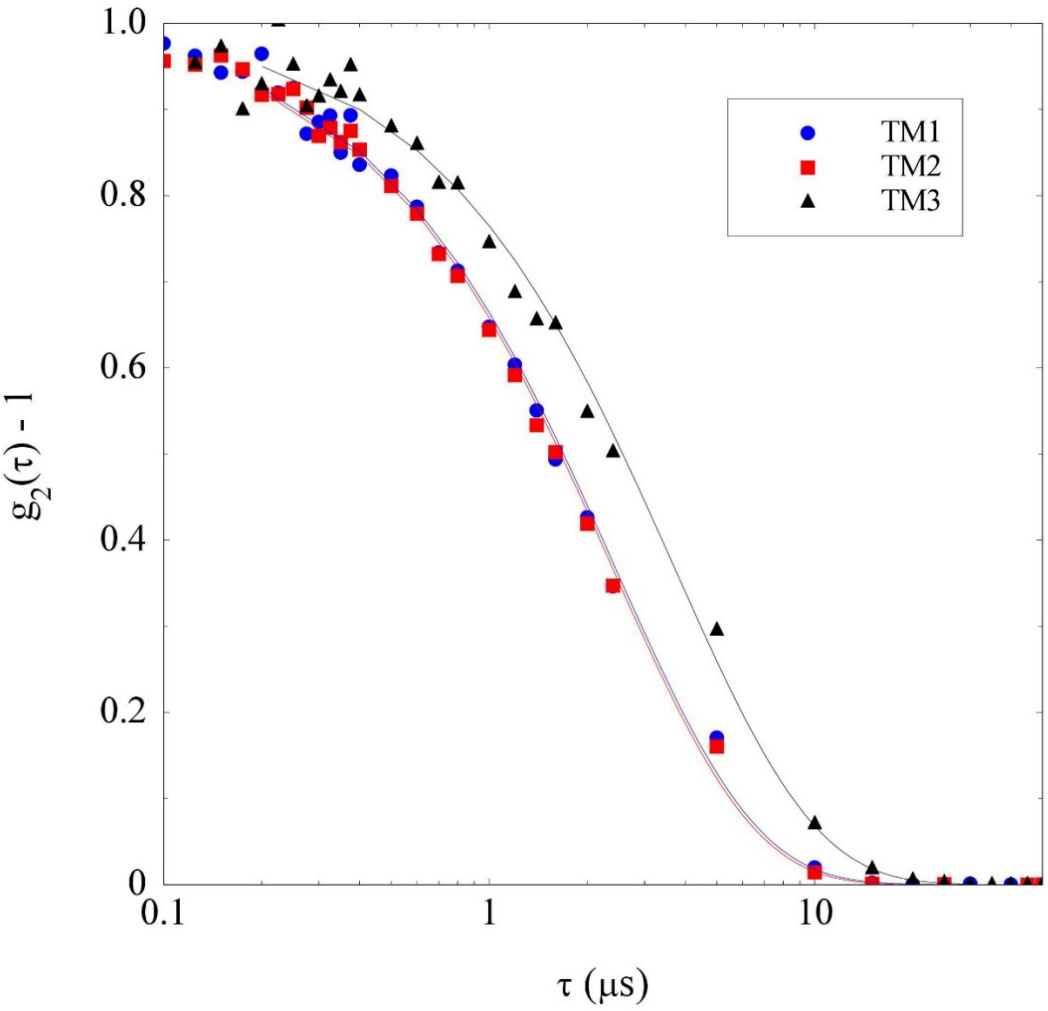

Figure 4. Intensity correlation functions $g_2\ (\tau)$ from the ternary solvents mixtures indicated in Table 1 fitted with single exponentials.

Considering the values for the solvent viscosities given in Table 1, these relaxation time yield a characteristic size (radius) for the scattering structures observed in solvents TM1, TM2, and TM3, of about 0.3, 0.5, and 0.8 nm respectively. One may guess that these values correspond to the correlation length ξ of the solvent, whose value could be enhanced by the presence of critical fluctuations. Within this interpretation, however, it is rather hard justifying that the largest value of ξ is obtained for the sample that is *farther* from the critical point (see Figure 1). Besides, appealing to a consistent contribution of the

critical fluctuations implies assuming that the coexistence curve is very close to the *spinodal* line bordering the region of thermodynamic instability of the mixture.

A possible alternative explanation is that the observed correlations are due to the so-called "pre-Ouzo effect", a self-aggregation effect that has been reported for a wide class of ternary mixtures composed by a “hydrotrope” (such as ethanol) and two mutually immiscible fluids (like water and DCB), both soluble in the hydrotrope in any proportions.[23,43,44] This peculiar phenomenon is named after the better known and widely investigated Ouzo effect, which amounts to the formation of rather monodisperse surfactant-free emulsions upon phase separation in ternary mixtures of the same kind. The crucial difference is that the pre-Ouzo effect, whose origin is still debated,[45,46] does not occur within the phase coexistence, but rather within the *stable* region of the phase diagram.

Distinguishing between these two different interpretations will necessarily require a more extensive investigation of the solvents we used, arguably by means of techniques allowing to explore a much wider range of scattering wave-vectors such as small-angle X or neutron scattering. Nevertheless, as discussed below, this anomalous scattering effect must be attentively considered in the analysis of the DLS correlation functions from the particle suspensions.

We now consider DLS measurements of the samples prepared in solvents TM1 and TM2 that, as discussed above, visual inspection suggests to be rather stable dispersions. The “bare” correlation functions originally obtained from the samples, were first cleared of the solvent contribution by focusing on the short-time behaviour of the *field* correlation function $g_1(\tau) = \sqrt{g_2(\tau) - 1}$. The latter was regarded as a linear combination of the decay due to the NPs plus a faster contribution due to the “nanodroplets” spontanouely occurring in the solvent using the droplet size obtained from the data in Figure 4. This numerical procedure allowed us to estimate a solvent contribution to $g_1(\tau)$ amounting from 20 % for the TM2 dispersion up to to 48% for the TM1 sample, which can then be accurately

subtracted out with the effect of modifying the decay rate of the correlation function on timescales shorter than a few tens of microseconds.

By taking into account the effect of the solvent viscosity on the decay of $g_2\ (\tau)$ and of its refractive index on the scattering wave-vector, these "corrected" intensity correlation functions can be directly compared with the correlation function obtained for the original aqueous NPs dispersion.

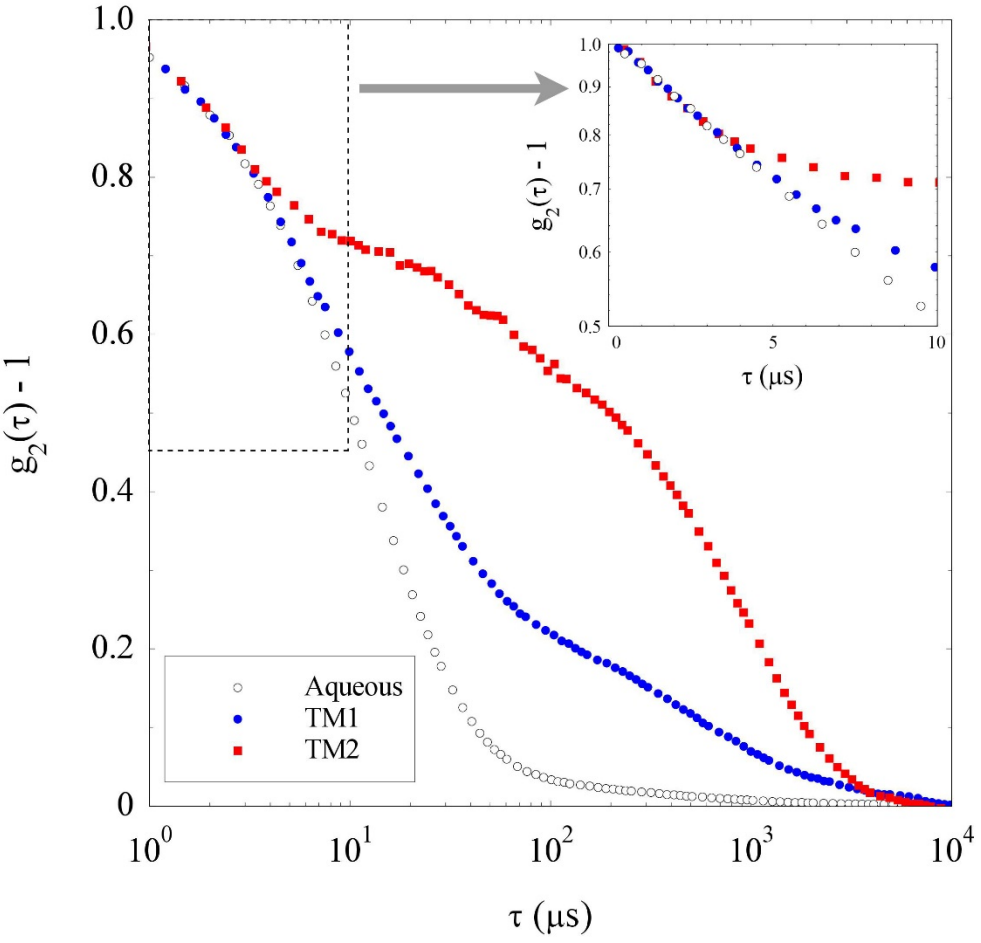

Figure 5. Intensity correlation functions of the zirconia dispersions in solvents TM1 (blue dots) and TM2 (red squares) obtained by subtracting the solvent contribution with their time axis rescaled as described in the text, compared to the correlation function for the nanoparticles in the original aqueous solvent (H_2O + 0.1 M HCl, open dots). The short-time region bounded by the dotted rectangle is expanded in the inset on a log *y*-scale.

Figure 5 shows that the three displayed correlation functions share a common general shape, characterized by a fast initial decrease followed by a much slower decay, whose fractional amplitude is very limited for the aqueous sample, but becomes consistently more relevant for the TM1 sample and becomes the dominant contribution for the dispersion in the TM2 mixture. This slow-decay component can be easily attributed to the presence of NPs' aggregates that were already detected for the original aqueous dispersion (see Figure 3), but that progressively get larger and arguably more numerous by exchanging the solvent to TM1 and, even more, TM2. The Figure 5 inset nevertheless shows that the short-time decay is basically identical for the three correlation functions, witnessing the persistence on non-aggregated NPs both in TM1 and TM2.

Given that the aggregate contribution is by far the dominant contribution to the decay of $g_2(\tau)$, one might however guess that the residual fraction of NPs, dispersed at their native dimensions, in sample TM2 is negligible. Yet, this first impression is fallacious, being essentially due to the strong dependence of the scattered intensity on the particle size. Indeed, provided that the NP clusters can be regarded as rather compact (namely, not tenuous fractal) objects of size R_c, their fractional contribution to the scattered intensity scales as $c_c R_c^3$, where c_c is the fraction of NPs aggregated into the clusters. As detailed in the SI, the typical cluster size and a rough evaluation of c_c can be obtained by considering the average relaxation time of $g_2(\tau)$, defined as the time-integral of the correlation function and by subtracting out the particle contribution (details are reported in SI section S4). The result of this approximate numerical analysis show that the cluster size progressively increases from $R_c \simeq 120$ nm in water to $R_c \gtrsim 300$ nm in both TM1 and TM2. However, even considering the approximation made in the evaluation, in both cases the fraction of particles associated in clusters is smaller than *one part over ten thousand* (Table S5).

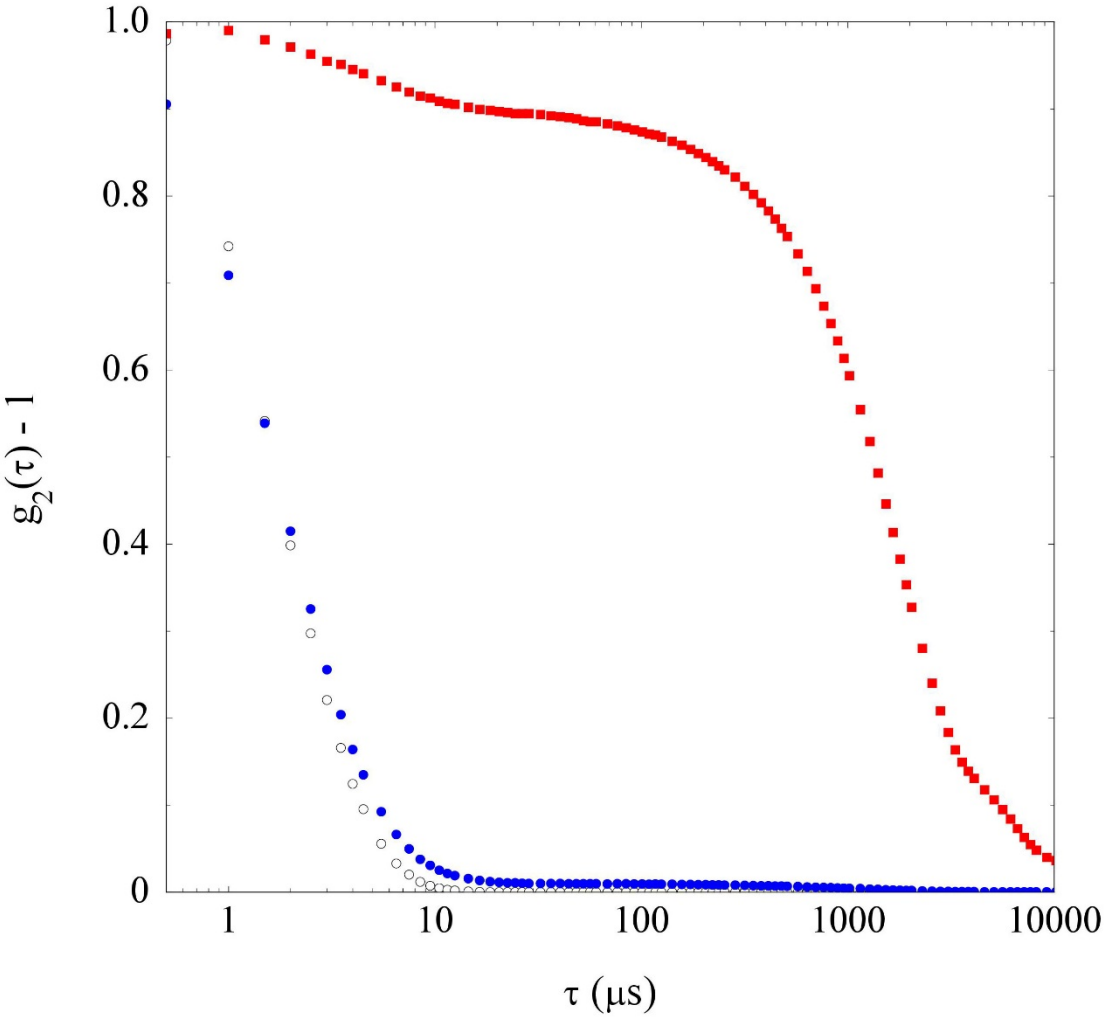

Figure 6. Intensity correlation functions of the zirconia dispersion in solvent TM3 just after preparation (red squares) and after filtration with a PTFE 0.1 μm filter (full dots), compared to the correlation function for the solvent mixture TM3 (open dots).

Measurements from the macroscopically unstable TM3 dispersion display a totally different scenario. Indeed, when a freshly prepared TM3 dispersion is fed into the light scattering cuvette without filtering, the DLS correlation function, shown in Figure 6, displays the presence of huge and rapidly settling aggregates, which are however almost completely removed by filtering, leaving an almost undetectable

amount of NPs in solution. We can then conclude that in solvent TM3 the Zirconia NPs undergo a rapid and complete colloidal aggregation process.

Summing up, DLS measurements show that the zirconia nanoparticles keep dispersed in their native size, with a tiny fraction of small aggregates up to a DCB weight fraction of about 60 % (solvent TM2) at least. This evidence is confirmed by TEM images (Figure 7), which display the presence of a large number of single ZrO_2 nanoparticles coexisting with small clusters composed by few particles, whereas bigger aggregates are rarely observed. Further increase of DCB to ω = 82 % leads however to the rapid growth of large aggregates incorporating almost all the individual nanoparticles.

While the achievement of stable dispersions of ZrO_2-NPs in organic solvents is rather easily achieved by the superficial modification of the nanoparticles, obtaining dispersions where the particles retain their native size is anything but trivial. At the same time, the stability of the dispersions is of great importance from an applicative point of view. In case of ZrO_2-NPs dispersed after surface functionalization, the stability of the dispersion can strictly depend on the kind and degree of grafting, and on the storing conditions. For instance, the stability of dispersions made of ZrO_2-NPs functionalized with vinyl group-containing ligands can encounter flocculation when the grafting degree is below a certain value or when stored in open vessel.[15]

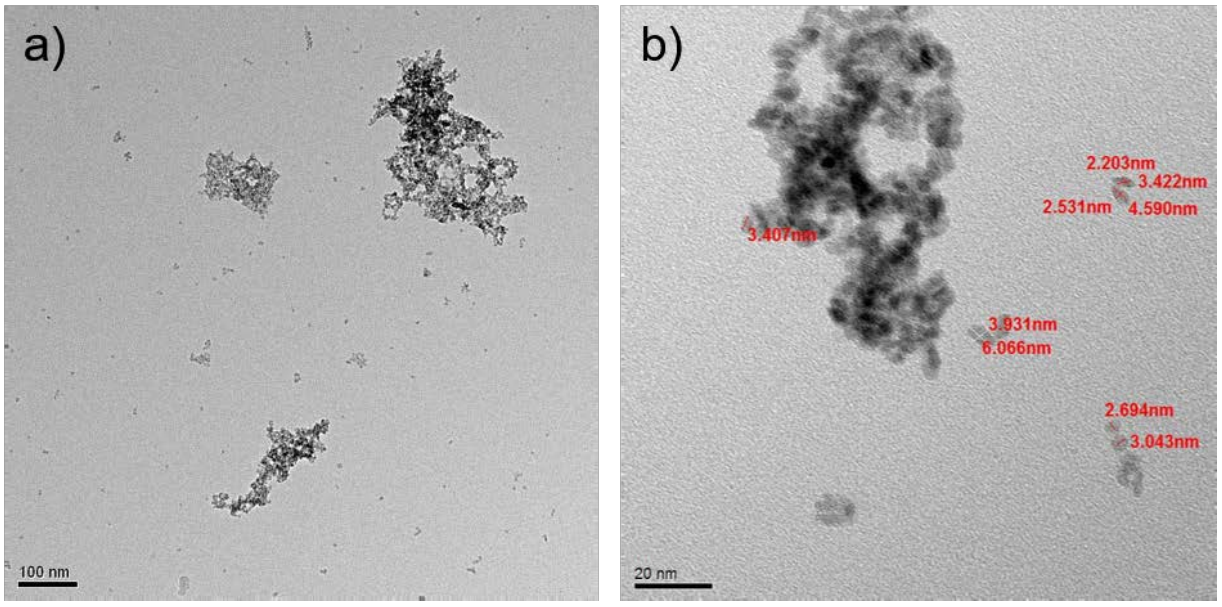

Figure 7. TEM images of sample TM2. Scale bar of a) and b) respectively 100 nm and 20 nm. A HR-TEM image is reported in Figure S14.

Outlook. Despite herein we are offering specific guidelines for the design of zirconia-based nanodispersion in 1,2-dichlorobenzene, the employed approach can be further extended to other systems. Indeed, thanks to the availability of the group-contribution parameters of many functional moieties, the UNIFAC-LLE model equations can be numerically solved for a high number of common solvents mixtures. Consequently, once a solvent able to disperse nanoparticles at the desired concentration is identified, this dispersion can be diluted with other solvents, which are theoretically unsuitable to achieve homogeneous dispersions, exploiting the information coming from the mixability diagrams computed with the UNIFAC-LLE model. As a first approximation, the model results can be validated qualitatively case by case by preparing different solvent mixtures and visually inspecting it. However, the behaviour of final dispersions in terms of aggregates dimensions cannot be easily predicted *a priori*. For example, in case of ZrO2-NPs dispersed in aqueous HCl the substitution of EtOH with acetone leads in all cases to nanoparticles aggregation and consequent precipitation (data not shown).

Conclusions

Zirconia nanoparticles were synthetized following a classic sol-gel approach widely reported in literature, and the achieved nanoparticles were characterized by means of X-ray diffraction and Raman spectroscopy. The synthetized ZrO_2-NPs resulted to have crystallite dimensions of about 4 nm and were a mixture of monoclinic and tetragonal phases (respectively 69 % and 31 %). These nanoparticles could be easily dispersed in aqueous HCl (0.1M) at their native dimensions, indeed DLS measurements showed particles with hydrodynamic diameter of about 5 nm.

Several applications of ceramic nanoparticles require their effective dispersion in an organic solvent, often immiscible with water. In this work, we overcame the use of additives employing a mixture of three different solvents. 1,2-dichlorobenzene is a chlorinated solvent which is generally immiscible with water, but by means of a polar co-solvent, like ethanol, it was possible to generate homogeneous ternary mixtures with water, when all the solvents are mixed in the proper amount. In order to predict which solvent ratios were able to form stable and homogeneous solutions, a ternary miscibility diagram of H_2O, ethanol and 1,2-dichlorobenzene mixtures was computed from UNIFAC-LLE model and was experimentally validated. DLS analysis highlighted that, when the mixtures are closed to the two-phase boundary, nanometric structures were formed, as in the case of surfactant-free microemulsions and, as far as we know, this result is reported for the first time for the three chosen solvents. The good accordance between the results computed from UNIFAC-LLE and the experimental results, also in presence of the presence of surfactant-free microemulsions, confirm once again the flexibility of this model. Then, the behaviour of the ZrO_2-NPs dispersed in the ternary mixtures were studied by means of DLS experiments, which indicated that the obtainment of nanoparticles dispersed at their native dimensions is possible when the DCB mass fraction was lower than 60 %. However, increasing of the amount of 1,2-

dichlorobenzene generally leads to rapid and complete nanoparticles aggregation, in particular when the mass fraction reaches values of about 80 %.

Thanks to the flexibility of the UNIFAC-LLE model, this approach can be easily extended to other ternary mixtures of solvents, in order to tune the solvent mixture according to the specific needs of the desired applications and can be used for nanoparticle dispersions by avoiding the addition of any other dispersant or further surface modifications.

Associated content

Supporting information

Details on UNIFAC model equations and UNIFAC-LLE parameters, details on mixtures prepared for the validation of the UNIFAC model, ^{1}H-NMR analysis, HR-TEM.

Author information

Corresponding Author

Andrea Fiorati - Politecnico di Milano, Department of Chemistry, Materials and Chemical Engineering "G. Natta" and INSTM - Local Unit Politecnico di Milano; orcid.org/0000-0002-2260-0563; Email: andrea.fiorati@polimi.it

Authors

Federico Florit - Politecnico di Milano, Department of Chemistry, Materials and Chemical Engineering "G. Natta"; orcid.org/ 0000-0002-6484-4953

Andrea Mazzei - Politecnico di Milano, Department of Chemistry, Materials and Chemical Engineering "G. Natta";

Stefano Buzzaccaro - Politecnico di Milano, Department of Chemistry, Materials and Chemical Engineering "G. Natta"; https://orcid.org/0000-0002-7394-5262

Barbara Rossi - Elettra Sincrotrone Trieste, Strada Statale 14 km 163.5, Area Science Park, 34149 Basovizza, Trieste, Italy and Department of Physics, University of Trento, Via Sommarive 14, 38123 Povo, Trento, Italy; orcid.org/0000-0003-1357-8074

Roberto Piazza - Politecnico di Milano, Department of Chemistry, Materials and Chemical Engineering “G. Natta”; orcid.org/0000-0001-7398-0335

Renato Rota - Politecnico di Milano, Department of Chemistry, Materials and Chemical Engineering “G. Natta”; orcid.org/0000-0002-3253-4424

Luigi De Nardo - Politecnico di Milano, Department of Chemistry, Materials and Chemical Engineering “G. Natta” and INSTM - Local Unit Politecnico di Milano; https://orcid.org/0000-0002-7492-6012

Funding Sources.

Andrea Fiorati and Luigi De Nardo thanks Regione Lombardia (POR-FESR 2014-2020 HOT & COLD ID 244823) for the financial support of the experimental activity of Andrea Fiorati.

Roberto Piazza and Stefano Buzzacaro acknowledge funding from the Italian Ministry for Education, University and Research (PRIN Project ID2017Z55KCW - `Soft Adaptive Networks').

Acknowledgments. The authors thanks: Francesca Broglia and Simone Gelosa for ICP-OES analysis, Mattia Ronchi for XRD measurements and Dr. Francesca Tana for the meaningful suggestions about the synthesis of Zirconia Nanoparticles.

References

(1) Garvie, R. C.; Hannink, R. H.; Pascoe, R. T. Ceramic Steel? *Nature* **1975**, *258* (5537), 703–704. https://doi.org/10.1038/258703a0.

(2) Tanabe, K. Surface and Catalytic Properties of ZrO2. *Mater. Chem. Phys.* **1985**, *13* (3–4), 347–364. https://doi.org/10.1016/0254-0584(85)90064-1.

(3) Wilk, G. D.; Wallace, R. M.; Anthony, J. M. High-κ Gate Dielectrics: Current Status and Materials Properties Considerations. *J. Appl. Phys.* **2001**, *89* (10), 5243–5275. https://doi.org/10.1063/1.1361065.

(4) Tana, F.; Serafini, A.; Lutterotti, L.; Cigada, A.; Variola, F.; Bondioli, F.; De Nardo, L. Particle Anisotropy and Crystalline Phase Transition in One-Pot Synthesis of Nano-Zirconia: A Causal Relationship. *CrystEngComm* **2018**, *20* (7), 879–888. https://doi.org/10.1039/c7ce01949a.

(5) Tana, F.; Messori, M.; Contini, D.; Cigada, A.; Valente, T.; Variola, F.; De Nardo, L.; Bondioli, F. Synthesis and Characterization of Scratch-Resistant Hybrid Coatings Based on Non-Hydrolytic Sol-Gel ZrO2 Nanoparticles. *Prog. Org. Coatings* **2017**, *103*, 60–68. https://doi.org/10.1016/j.porgcoat.2016.11.022.

(6) Wang, Z.; Lu, Y.; Yuan, S.; Shi, L.; Zhao, Y.; Zhang, M.; Deng, W. Hydrothermal Synthesis and Humidity Sensing Properties of Size-Controlled Zirconium Oxide (ZrO2) Nanorods. *J. Colloid Interface Sci.* **2013**, *396*, 9–15. https://doi.org/10.1016/J.JCIS.2012.12.068.

(7) Tonbul, Y.; Akbayrak, S.; Özkar, S. Nanozirconia Supported Ruthenium(0) Nanoparticles: Highly Active and Reusable Catalyst in Hydrolytic Dehydrogenation of Ammonia Borane. *J. Colloid Interface Sci.* **2018**, *513*, 287–294. https://doi.org/10.1016/J.JCIS.2017.11.037.

(8) Fernández-García, M.; Martínez-Arias, A.; Hanson, J. C.; Rodriguez, J. A. Nanostructured Oxides in Chemistry: Characterization and Properties. *Chem. Rev.* **2004**, *104* (9), 4063–4104. https://doi.org/10.1021/cr030032f.

(9) Cheema, T. A.; Garnweitner, G. Phase-Controlled Synthesis of ZrO2 Nanoparticles for Highly Transparent Dielectric Thin Films. *CrystEngComm* **2014**, *16* (16), 3366–3375. https://doi.org/10.1039/C3CE42392A.

(10) Garvie, R. C. Stabilization of the Tetragonal Structure in Zirconia Microcrystals. *J. Phys. Chem.* **1978**, *82* (2), 218–224. https://doi.org/10.1021/j100491a016.

(11) Witten, T. A.; Witten, T.; Pincus, P. A.; Pincus, P. *Structured Fluids: Polymers, Colloids, Surfactants*; Oxford University Press on Demand, 2004, 232.

(12) Zhang, W. Nanoparticle Aggregation: Principles and Modeling. In *Nanomaterial*; Springer, 2014; pp 19–43.

(13) Grote, C.; Cheema, T. A.; Garnweitner, G. Comparative Study of Ligand Binding during the Postsynthetic Stabilization of Metal Oxide Nanoparticles. *Langmuir* **2012**, *28* (40), 14395–14404. https://doi.org/10.1021/la301822r.

(14) Luo, K.; Zhou, S.; Wu, L.; Gu, G. Dispersion and Functionalization of Nonaqueous Synthesized Zirconia Nanocrystals via Attachment of Silane Coupling Agents. *Langmuir* **2008**, *24* (20), 11497–11505. https://doi.org/10.1021/la801943n.

(15) Zhou, S.; Garnweitner, G.; Niederberger, M.; Antonietti, M. Dispersion Behavior of Zirconia Nanocrystals and Their Surface Functionalization with Vinyl Group-Containing Ligands. *Langmuir* **2007**, *23* (18), 9178–9187. https://doi.org/10.1021/la700837u.

(16) Scholz, S.; Kaskel, S. Surface Functionalization of ZrO2 Nanocrystallites for the Integration into Acrylate Nanocomposite Films. *J. Colloid Interface Sci.* **2008**, *323* (1), 84–91. https://doi.org/10.1016/J.JCIS.2008.03.051.

(17) Wang, S.-H.; Liu, J.-H.; Pai, C.-T.; Chen, C.-W.; Chung, P.-T.; Chiang, A. S.-T.; Chang, S.-J. Hansen Solubility Parameter Analysis on the Dispersion of Zirconia Nanocrystals. *J. Colloid Interface Sci.* **2013**, *407*, 140–147. https://doi.org/10.1016/J.JCIS.2013.07.001.

(18) Wang, S.-H.; Sun, Y.-S.; Chiang, A. S.-T.; Hung, H.-F.; Chen, M.-C.; Wood, K. Carboxylic Acid-Directed Clustering and Dispersion of ZrO2 Nanoparticles in Organic Solvents: A Study by Small-Angle X-Ray/Neutron Scattering and NMR. *J. Phys. Chem. C* **2011**, *115* (24), 11941–11950. https://doi.org/10.1021/jp202243z.

(19) Bijlard, A.-C.; Wald, S.; Crespy, D.; Taden, A.; Wurm, F. R.; Landfester, K. Functional Colloidal Stabilization. *Adv. Mater. Interfaces* **2017**, *4* (1), 1600443. https://doi.org/10.1002/admi.201600443.

(20) Fengqiu, T.; Xiaoxian, H.; Yufeng, Z.; Jingkun, G. Effect of Dispersants on Surface Chemical Properties of Nano-Zirconia Suspensions. *Ceram. Int.* **2000**, *26* (1), 93–97. https://doi.org/10.1016/S0272-8842(99)00024-3.

(21) Enomoto, K.; Kikuchi, M.; Narumi, A.; Kawaguchi, S. Surface Modifier-Free Organic–Inorganic Hybridization To Produce Optically Transparent and Highly Refractive Bulk Materials Composed of Epoxy Resins and ZrO2 Nanoparticles. *ACS Appl. Mater. Interfaces* **2018**, *10* (16), 13985–13998. https://doi.org/10.1021/acsami.8b00422.

(22) Moloney, V. M. B.; Parris, D.; Edirisinghe, M. J. Rheology of Zirconia Suspensions in a Nonpolar Organic Medium. *J. Am. Ceram. Soc.* **1995**, *78* (12), 3225–3232. https://doi.org/10.1111/j.1151-2916.1995.tb07958.x.

(23) Kunz, W.; Holmberg, K.; Zemb, T. Hydrotropes. *Curr. Opin. Colloid Interface Sci.* **2016**, *22*, 99–107. https://doi.org/https://doi.org/10.1016/j.cocis.2016.03.005.

(24) Schöttl, S.; Marcus, J.; Diat, O.; Touraud, D.; Kunz, W.; Zemb, T.; Horinek, D. Emergence of Surfactant-Free Micelles from Ternary Solutions. *Chem. Sci.* **2014**, *5* (8), 2949–2954. https://doi.org/10.1039/C4SC00153B.

(25) Schöttl, S.; Horinek, D. Aggregation in Detergent-Free Ternary Mixtures with Microemulsion-like Properties. *Curr. Opin. Colloid Interface Sci.* **2016**, *22*, 8–13. https://doi.org/https://doi.org/10.1016/j.cocis.2016.02.003.

(26) Lopian, T.; Schöttl, S.; Prévost, S.; Pellet-Rostaing, S.; Horinek, D.; Kunz, W.; Zemb, T. Morphologies Observed in Ultraflexible Microemulsions with and without the Presence of a Strong Acid. *ACS Cent. Sci.* **2016**, *2* (7), 467–475. https://doi.org/10.1021/acscentsci.6b00116.

(27) Schöttl, S.; Matubayasi, N.; Horinek, D. Solubilization Power of Surfactant-Free Microemulsions. *Phys. Chem. Chem. Phys.* **2020**, *22* (39), 22185–22189. https://doi.org/10.1039/D0CP02933E.

(28) Fredenslund, A.; Jones, R. L.; Prausnitz, J. M. Group-Contribution Estimation of Activity Coefficients in Nonideal Liquid Mixtures. *AIChE J.* **1975**, *21* (6), 1086–1099. https://doi.org/10.1002/aic.690210607.

(29) Renon, H.; Prausnitz, J. M. Local Compositions in Thermodynamic Excess Functions for Liquid Mixtures. *AIChE J.* **1968**, *14* (1), 135–144. https://doi.org/10.1002/aic.690140124.

(30) Abrams, D. S.; Prausnitz, J. M. Statistical Thermodynamics of Liquid Mixtures: A New Expression for the Excess Gibbs Energy of Partly or Completely Miscible Systems. *AIChE J.* **1975**, *21* (1), 116–128. https://doi.org/10.1002/aic.690210115.

(31) Onken, U.; Rarey-Nies, J.; Gmehling, J. The Dortmund Data Bank: A Computerized System for Retrieval, Correlation, and Prediction of Thermodynamic Properties of Mixtures. *Int. J.*

Thermophys. **1989**, *10* (3), 739–747. https://doi.org/10.1007/BF00507993.

(32) Skjold-Jorgensen, S.; Kolbe, B.; Gmehling, J.; Rasmussen, P. Vapor-Liquid Equilibria by UNIFAC Group Contribution. Revision and Extension. *Ind. Eng. Chem. Process Des. Dev.* **1979**, *18* (4), 714–722. https://doi.org/10.1021/i260072a024.

(33) Magnussen, T.; Rasmussen, P.; Fredenslund, A. Unifac Parameter Table for Prediction of Liquid-Liquid Equilibria. *Ind. Eng. Chem. Process Des. Dev.* **1981**, *20* (2), 331–339. https://doi.org/10.1021/i200013a024.

(34) Gottlieb, H. E.; Kotlyar, V.; Nudelman, A. NMR Chemical Shifts of Common Laboratory Solvents as Trace Impurities. *J. Org. Chem.* **1997**, *62* (21), 7512–7515. https://doi.org/10.1021/jo971176v.

(35) Furasova, A. D.; Ivanovski, V.; Yakovlev, A. V.; Milichko, V. A.; Vinogradov, V. V.; Vinogradov, A. V. Inkjet Fabrication of Highly Efficient Luminescent Eu-Doped ZrO 2 Nanostructures. *Nanoscale* **2017**, *9* (35), 13069–13078. https://doi.org/10.1039/c7nr03175k.

(36) Gambe, J.; Rémondière, F.; Jouin, J.; Portal, L.; Thomas, P.; Masson, O. Detrimental Effect and Neutralization of in Situ Produced Water on Zirconia Nanoparticles Obtained by a Nonaqueous Sol-Gel Method. *Inorg. Chem.* **2019**, *58* (22), 15175–15188. https://doi.org/10.1021/acs.inorgchem.9b02076.

(37) Rossberg, M.; Lendle, W.; Pfleiderer, G.; Tögel, A.; Dreher, E.-L.; Langer, E.; Rassaerts, H.; Kleinschmidt, P.; Strack, H.; Cook, R.; et al. Chlorinated Hydrocarbons. *Ullmann's Encyclopedia of Industrial Chemistry*. July 15, 2006. https://doi.org/doi:10.1002/14356007.a06_233.pub2.

(38) Garnweitner, G.; Goldenberg, L. M.; Sakhno, O. V.; Antonietti, M.; Niederberger, M.; Stumpe, J.

Large-Scale Synthesis of Organophilic Zirconia Nanoparticles and Their Application in Organic–Inorganic Nanocomposites for Efficient Volume Holography. *Small* **2007**, *3* (9), 1626–1632. https://doi.org/10.1002/smll.200700075.

(39) Doebelin, N.; Kleeberg, R. Profex: A Graphical User Interface for the Rietveld Refinement Program BGMN. *J. Appl. Crystallogr.* **2015**, *48* (5), 1573–1580. https://doi.org/10.1107/S1600576715014685.

(40) Zhong, L.; Chen, X.; Song, H.; Guo, K.; Hu, Z. Synthesis of Monolithic Zirconia Aerogel via a Nitric Acid Assisted Epoxide Addition Method. *RSC Adv.* **2014**, *4* (60), 31666–31671. https://doi.org/10.1039/C4RA04601C.

(41) Fernández López, E.; Sánchez Escribano, V.; Panizza, M.; Carnasciali, M. M.; Busca, G. Vibrational and Electronic Spectroscopic Properties of Zirconia Powders. *J. Mater. Chem.* **2001**, *11* (7), 1891–1897. https://doi.org/10.1039/B100909P.

(42) Philippi, C. M.; Mazdiyasni, K. S. Infrared and Raman Spectra of Zirconia Polymorphs. *J. Am. Ceram. Soc.* **1971**, *54* (5), 254–258. https://doi.org/10.1111/j.1151-2916.1971.tb12283.x.

(43) Diat, O.; Klossek, M. L.; Touraud, D.; Deme, B.; Grillo, I.; Kunz, W.; Zemb, T. Octanol-Rich and Water-Rich Domains in Dynamic Equilibrium in the Pre-Ouzo Region of Ternary Systems Containing a Hydrotrope. *J. Appl. Crystallogr.* **2013**, *46* (6), 1665–1669. https://doi.org/10.1107/S002188981302606X.

(44) Klossek, M. L.; Touraud, D.; Zemb, T.; Kunz, W. Structure and Solubility in Surfactant-Free Microemulsions. *ChemPhysChem* **2012**, *13* (18), 4116–4119. https://doi.org/https://doi.org/10.1002/cphc.201200667.

(45) Zemb, T. N.; Klossek, M.; Lopian, T.; Marcus, J.; Schöettl, S.; Horinek, D.; Prevost, S. F.; Touraud, D.; Diat, O.; Marčelja, S.; et al. How to Explain Microemulsions Formed by Solvent Mixtures without Conventional Surfactants. *Proc. Natl. Acad. Sci.* **2016**, *113* (16), 4260 LP – 4265. https://doi.org/10.1073/pnas.1515708113.

(46) Shimizu, S.; Matubayasi, N. Hydrotropy and Scattering: Pre-Ouzo as an Extended near-Spinodal Region. *Phys. Chem. Chem. Phys.* **2017**, *19* (39), 26734–26742. https://doi.org/10.1039/C7CP04990K.